


## Research Article

# Automatic Classification System of Drainage Hole Blockage Based on Convolution Neural Network Transfer Learning

Jianbing Lv,<sup>1</sup> Weijun Wu,<sup>1</sup> Xiaoyu Kang,<sup>1</sup> Juan Huang ,<sup>1</sup> Gongfa Chen,<sup>1</sup> Shuai Teng,<sup>1</sup> and Hejie Gao<sup>2</sup>

<sup>1</sup>School of Civil and Transportation Engineering, Guangdong University of Technology, Guangzhou 510006, China

<sup>2</sup>CCCC Fourth Navigation Engineering Bureau Co., LTD., Guangzhou 510000, China

Correspondence should be addressed to Juan Huang; [cvjuanhuang@gdut.edu.cn](mailto:cvjuanhuang@gdut.edu.cn)

Received 22 February 2022; Revised 9 April 2022; Accepted 10 May 2022; Published 15 July 2022

Academic Editor: Nhat-Duc Hoang

Copyright © 2022 Jianbing Lv et al. This is an open access article distributed under the Creative Commons Attribution License, which permits unrestricted use, distribution, and reproduction in any medium, provided the original work is properly cited.

The blockage or failure of the drainage holes will endanger the stability of the slopes and traffic safety of a highway tunnel. This paper studies an algorithm for the automatic classification of drainage hole blockage degree based on convolutional neural network transfer learning to explore the intelligent detection method of drainage hole blockage. The model transfer method is adopted to input drainage hole image samples to retrain the pretrained network to classify new images. Experiments are performed on the collected samples of drainage hole images, and the accuracy of different network models is compared, ResNet-18 being the best. The ResNet-18 performance is compared using different transfer strategies and parameters. The results show that when the SGDM gradient optimisation algorithm is used and the learning rate is 0.0001, the identification effect of these samples is the best. The validation accuracy can reach 91.7%, test accuracy is 90.0%, and the effective classification of drainage hole blockage to different degrees is realised under the transfer learning strategy of ResNet-18 model 1–34 frozen layers. Furthermore, with an expansion of the samples in the future, the identification accuracy will be further improved. The automatic classification system of the blockage degree of drainage hole greatly reduces the cost of manual detection, plays a guiding role in the maintenance of drainage pipes, and effectively improves the safety of highway tunnels and slopes.

## 1. Introduction

With the continued extension of tunnels to mountains and offshore deepwater areas, a series of complex diseases have emerged in both tunnels under construction and in operation [1]. Severe crystal blockage of tunnel drainage pipes generally occurs during tunnel construction and operation. After the drainage pipes become clogged, the depressurisation capacity will be greatly weakened, which will easily lead to the inability of tunnel groundwater to be drained and a sudden rise in external water pressure [2]. This causes structural water leakage, cracked lining and damaged blocks, inverted arch uplift, and other diseases [3–5], all of which have a serious impact on the tunnel structure's safe operation, ranging from road blockage to casualties. To effectively avoid the occurrence of tunnel disasters caused by the blockage of the drainage holes, it is necessary to conduct

rapid and accurate inspections of the drainage holes regularly. Currently, the tunnel drainage hole blockage detection relies primarily on visual inspection and recording by inspectors on the spot, followed by maintenance by maintenance personnel. The inspection results are subjectively affected by the inspectors. The inspection tasks in the tunnel are challenging, and the workload is heavy. Because false detection and missed detection often occur, it is urgent to explore an intelligent detection method.

Computer vision-based methods can intuitively and effectively detect structural damage, image binarisation [6], and edge detection [7]. Two methods have been widely used in vision-based structural health monitoring. Ho [8] et al. proposed a method for dynamic displacement measurement of infrastructure based on multipoint vision. Ye [9, 10] et al. proposed a long-distance noncontact distributed structural displacement monitoring method for large-span bridges

based on computer vision, which is also based on digital image processing correlation theory and multipoint template matching algorithm, and realised the kilometre-scale on-site structural displacement monitoring. However, this method still suffers from limitations due to the effects of illumination and distortion-induced noise [11]. Structure damage detection methods based on deep learning have been rapidly developed in the field of civil engineering, given the rapid advancement of artificial intelligence technology [12, 13]. Yeum et al. [14] proposed a vision-based bridge crack detection technology through automatic processing of object detection and grouping. Makantasis et al. [15] achieved tunnel crack detection by employing a shallow convolutional neural network (CNN) with two convolutional layers and one fully connected layer. Cha et al. [16] used a CNN deep structure to detect concrete cracks. Xu et al. [17] established a framework for surface crack identification of steel structures based on the restricted Boltzmann machine. Chen [18] proposed a CNN crack detection method based on naive Bayesian data fusion to improve the overall performance and robustness of the recognition algorithm. Bao et al. [19] proposed an abnormal data diagnosis method for structural health monitoring based on computer vision and deep networks. Konovalenk et al. [20] evaluated the application of residual neural networks in the identification of three types of industrial steel defects and researched and developed a model of rolling steel surface defect identification and classification based on deep residual neural network. Xue et al. [21] proposed an improved mask-RCNN (region-based CNN) model to realise automatic detection of tunnel lining leakage. In the drainage pipeline system disease detection, a defect classification system of sewer pipeline systems on closed-circuit television (CCTV) inspection videos based on CNN is proposed [22–24]. However, no research has been conducted on an automatic method for detecting the degree of slope in drainage hole blockage.

In this paper, deep learning is applied to detect blockages in drainage holes. As shown in Figure 1, many drainage hole disease samples were collected and taken as input. By comparing different pretrained CNNs, the CNN model most suitable for these samples was selected. By comparing the performance of the model under different migration strategies (freezing different layers) and the influence of different network hyperparameters on the network prediction effect, a CNN model, which is most suitable for the experimental samples, is finally obtained. In this paper, the automatic classification method of the blockage degree of drainage holes is proposed for the first time. The method combining transfer learning and CNN is adopted to overcome the shortcomings of training traditional CNNs, such as insufficient samples and long training time, and to realise automatic classification of the blockage degree of drainage holes while avoiding the defects of manual detection, such as high cost, long time, error detection, and leak detection.

Section 2 introduces the collection of experimental samples and image preprocessing, as well as pretraining models and transfer learning methods. Section 3.1 shows the results of transfer learning for different pretraining models.

Section 3.2 compares ResNet-18 under different transfer strategies. Section 3.3 compares the effects of different network hyperparameters on the prediction performance of the model. Section 3.4 presents the visualisation results of the convolutional process of a CNN. Section 4 shows the conclusion and prospects of this paper.

## 2. Experimental Data and Network Model

In this paper, the drainage hole blockage detection model retrains a pretrained CNN to classify a new set of images by using a model transfer learning method. Compared with training the network from the start with randomly initialised weights, fine-tuning the network through transfer learning is faster and simpler, owing to the transfer learning network's excellent feature extraction and classification capabilities. Fine-tuning the network through transfer learning is faster and easier than training the network from scratch with randomly initialised weights, and the learned features can be quickly transferred to new tasks with a smaller number of training images, resulting in efficient and accurate classification and detection of drainage hole blockage diseases. Figure 2 shows the detection process of the automatic detection model of drainage hole blockage.

*2.1. Experimental Data Preprocessing.* The original samples of this experiment were personally shot in the tunnel and slope because there are no public samples on the blockage of drainage holes on the Internet. The proportion of picture target and background is quite different, owing to the influence of shooting angle, drainage hole position and other factors. As a result, the image must be preprocessed. First, the collected image samples are appropriately cropped, and the size is uniformly scaled to adapt to the input size of the network ( $224 \times 224$ ). Additionally, in the process of training the network, image enhancement techniques of translation and rotation are used to enhance the robustness of the network and improve the generalisation ability of the network.

All pictures were manually classified, and qualitative analysis was carried out according to the degree of blockage. Furthermore, the blockage of drainage holes was divided into four categories, namely, slight blockage, moderate blockage, heavy blockage, and no blockage. Slight blockage occurs when the blockage crystallisation of drainage holes is less than about 1/4 of the drainage hole area, moderate blockage occurs when the blockage crystallisation is greater than about 1/4 but less than 3/4, and heavy blockage occurs when the blockage crystallisation is greater than about 3/4. Figure 3 depicts the exact classification.

A total of 943 samples were used in this experiment, 101 of which were taken as test sets. The remaining 842 samples were 299 with slight blockage, 230 with moderate blockage, 71 with heavy blockage, and 242 with no blockage. Approximately 90% (758) were randomly selected as training and 10% (84) as the validation set. Table 1 presents the allocation of the specific sample.

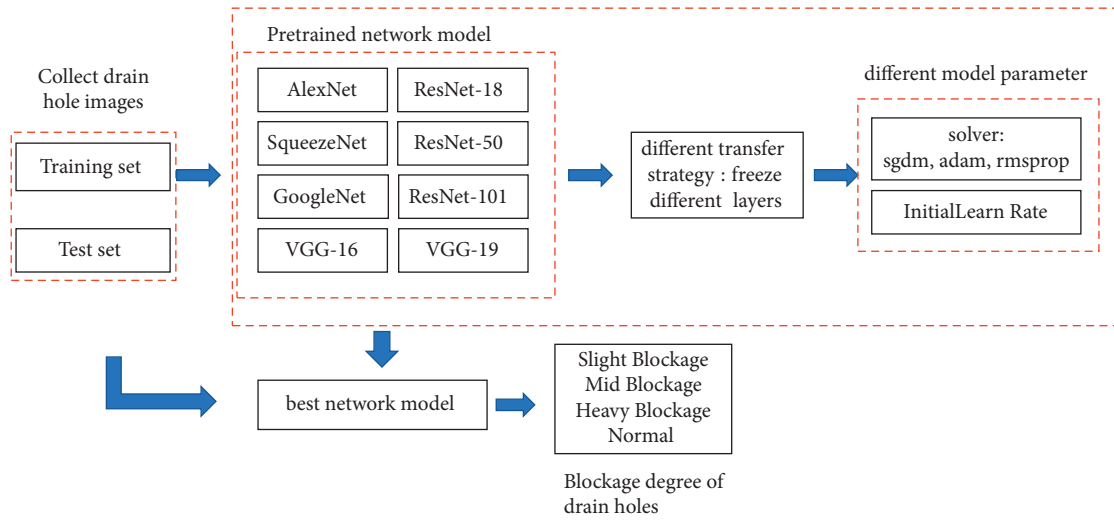


FIGURE 1: Technical route.

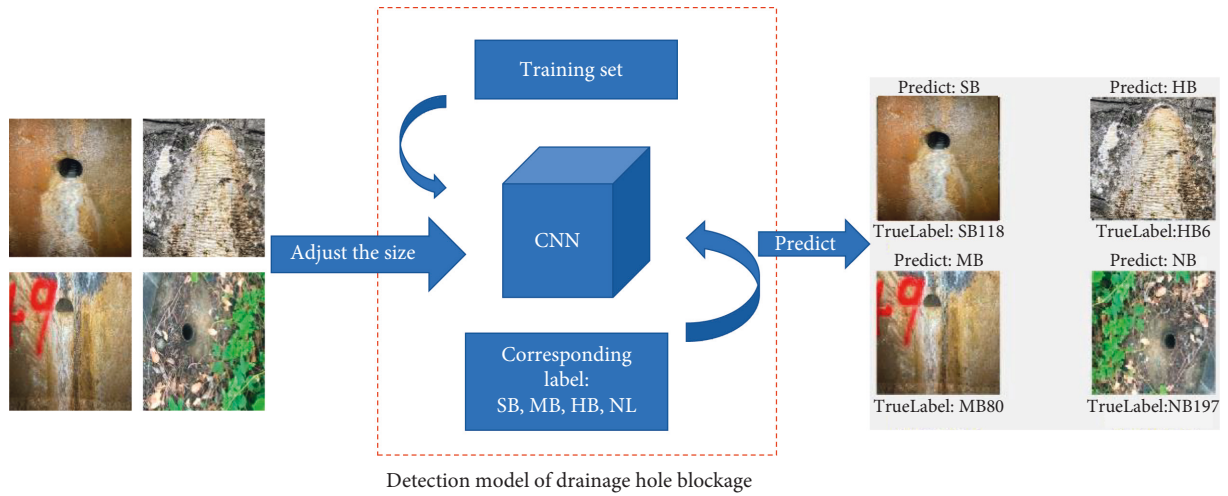


FIGURE 2: The detection process of the network model for blockage of drainage holes.

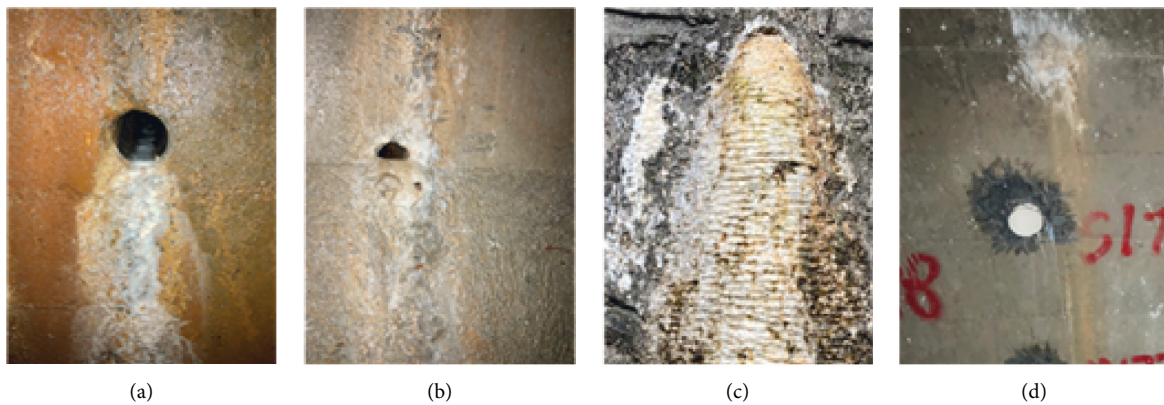


FIGURE 3: Drainage hole classification. (a) Slight blockage; (b) moderate blockage; (c) heavy blockage; (d) no blockage.

TABLE 1: Sample allocation.

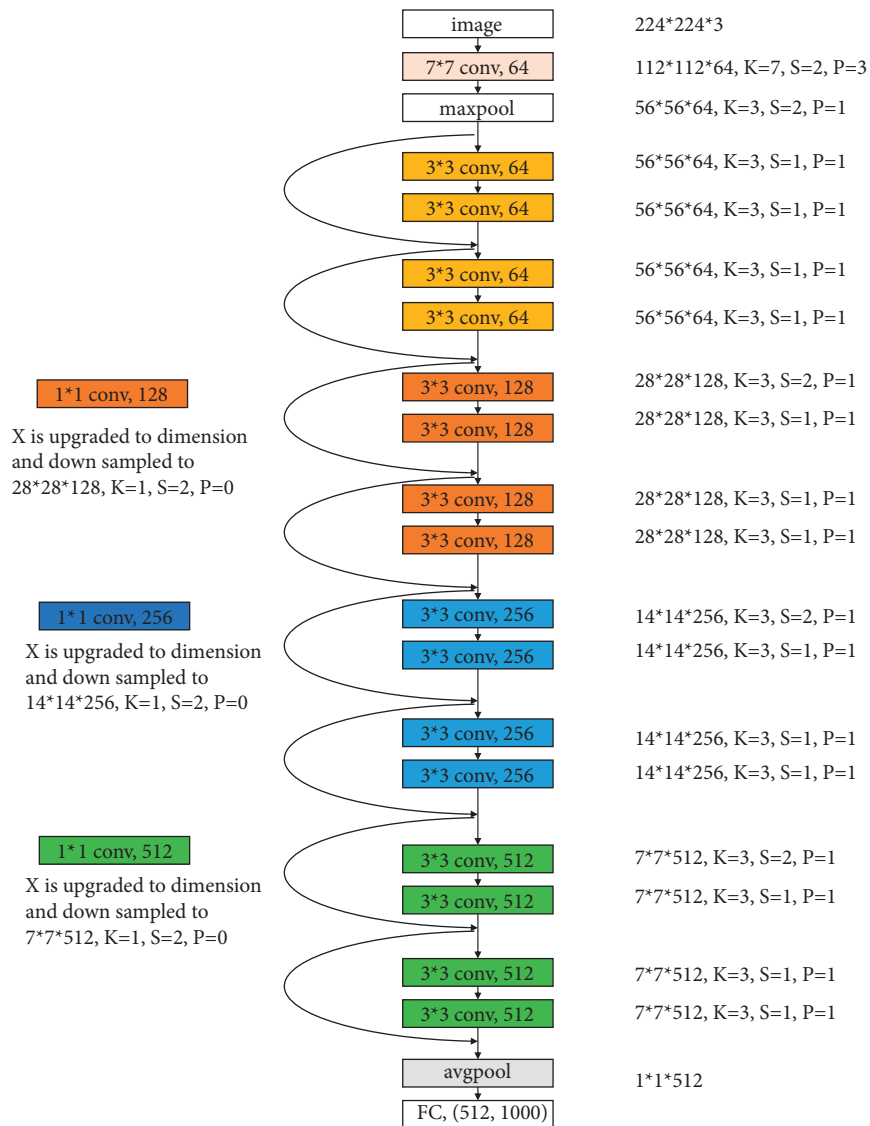
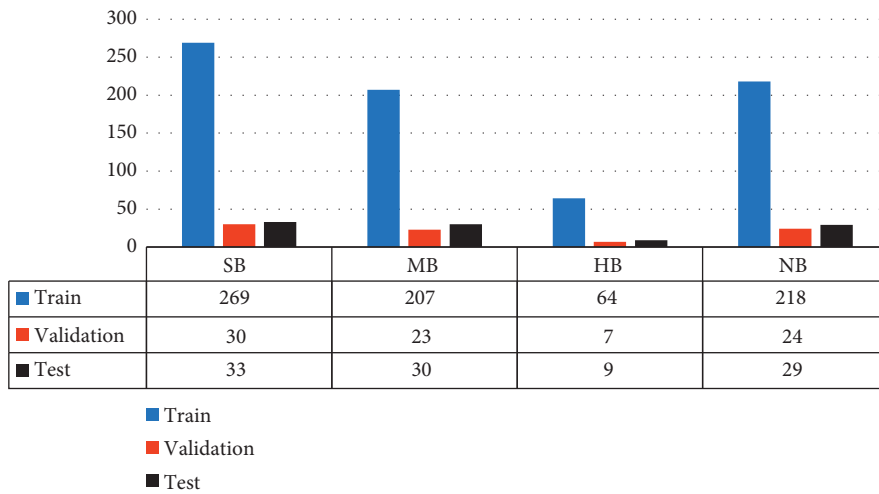


FIGURE 4: Network structure of the ResNet-18 model. Conv# = convolution; pool# = pooling; FC = full connection.

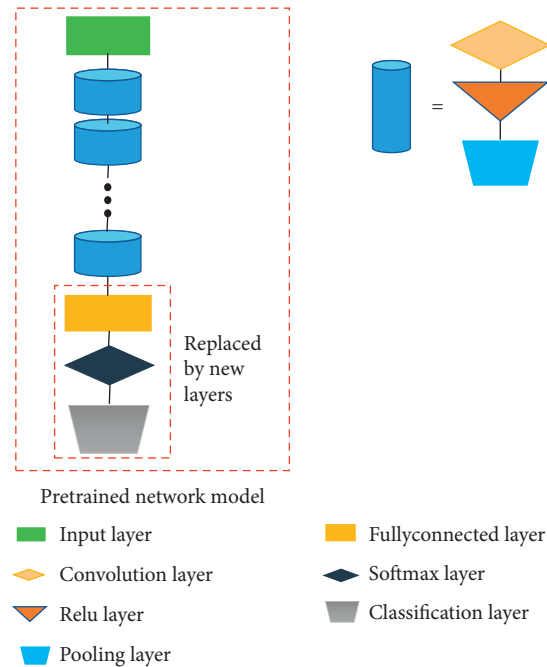


FIGURE 5: Model-based transfer learning.

**2.2. Model Transfer Learning Method.** CNN is a feedforward neural network that first appeared in the BP [25] algorithm in 1986. Compared with ordinary neural networks, it has the advantages of partial connection and weight sharing and is applied in the field of image recognition and target classification. In this paper, eight classical CNN models (AlexNet [26], SqueezeNet [27], VGG-16 [28], VGG-19, Resnet-18 [29], ResNet-50, ResNet-101, and GoogLeNet [30]) were selected as pretraining network models. All CNN models are composed of convolutional layers, activation layers, pooling layers, and fully connected layers. On the other hand, stacking layers make it difficult to improve the model's learning ability and cause model degradation and gradient explosion [31] or disappearance. Unlike other networks, ResNet uses shortcut connections to solve the problem of model degradation in deep neural networks, as shown in Figure 4. Adding an identity map behind the shallow network with equal input and output improves accuracy and transforms the model into a shallow network while improving the accuracy of the model.

The pretrained network has been trained on over one million images and can classify images into 1000 object categories, including keyboard, mouse, pencil, and many animals, as well as images of civil engineering. As a result, the network has learned rich feature representations for a range of different images. Since the three last layers of the pre-trained network are configured for 1000 classes, these three layers must be fine-tuned for our new classification problem, as shown in Figure 5. All but the last three layers are extracted from the pretrained network. By replacing the last three layers with new fully connected layers, softmax and classification layers, the fully connected layer is set to the same size as the number of classes in the new data, which is four for these experimental samples. In most networks, the

last layer with learnable weights is fully connected. In SqueezeNet, the last learnable layer is a  $1 \times 1$  convolutional layer, which is replaced by a new convolutional layer with the same number of filters as the number of classes.

### 3. Analysis of Results

The experimental platforms used in this article are as follows: Microsoft Windows 10 (operating system), i5-1035G1 central processing unit (CPU), NVIDIA GeForce MX350 8 GB graphics processing unit (GPU), 512 GB solid-state drive, and Matlab R2020a.

**3.1. Network Model Comparison.** All network models use the same network parameters with the specific parameters presented in Table 2. All network layers are trained, and the experimental results are comprehensively evaluated with four evaluation metrics, namely, validation accuracy, precision, recall, and F1-score.

This paper selects the validation set to evaluate the network, which contains 143 images, 30 of which are slight blockage, 23 are moderate blockage, 7 are heavy blockage, and 24 are no blockage. Different network models are compared in terms of validation accuracy, precision, recall, F1-score, test accuracy, and training time. Table 3 presents the performance of each network model. Figure 6 shows the training and validation accuracy, as well as the loss iteration curves during the training process. As can be observed, SqueezeNet has the shortest training time while having the lowest validation accuracy. The accuracy of the VGG-16/19 network is higher, but it takes a long time, and the test accuracy of VGG-19 is lower than the validation accuracy, resulting in overfitting. As the depth of the ResNet series

TABLE 2: Parameter setting.

Parameter	Value
Solver	sgdm
MaxEpoch	20
miniBatchsize	10
InitialLearnRate	0.0001
ValidationFrequency	5

TABLE 3: Network model performance comparison.

Network	Classify	Accuracy (ACC)	Precision (PPV) (%)	Recall (TPR) (%)	F 1-score (%)	Test accuracy (%)	Time
AlexNet	SB	88.1	85.3	96.7	0.91	89.1	6 m 10 s
	MB		90.9	87.0	0.89		
	HB		83.3	71.4	0.77		
	NB		90.9	83.3	0.87		
ResNet-18	SB	90.5	93.1	90.0	0.92	91.0	8 m 40 s
	MB		91.3	91.3	0.91		
	HB		71.4	71.4	0.71		
	NB		92.0	95.8	0.94		
ResNet-50	SB	85.8	82.5	88.9	0.86	90.0	36 m 59 s
	MB		93.4	82.6	0.88		
	HB		73.9	81.0	0.77		
	NB		87.5	86.3	0.87		
ResNet-101	SB	84.5	80.0	80.0	0.80	86.0	353 m 42 s
	MB		94.4	73.9	0.83		
	HB		77.8	100.0	0.88		
	NB		85.2	95.8	0.90		
GoogLeNet	SB	88.1	75.0	100.0	0.86	88.0	13 m 15 s
	MB		100.0	69.6	0.82		
	HB		100.0	85.7	0.92		
	NB		100.0	91.7	0.96		
VGG-16	SB	86.9	86.7	86.7	0.87	93.0	421 m 11 s
	MB		90.0	78.3	0.84		
	HB		58.3	100.0	0.74		
	NB		100.0	91.7	0.96		
VGG-19	SB	90.5	80.6	96.7	0.88	92.0	417 m 30 s
	MB		94.7	78.3	0.86		
	HB		100.0	100.0	1.00		
	NB		100.0	91.7	0.96		
SqueezeNet	SB	82.1	85.2	76.7	0.81	91.0	5 m 33 s
	MB		80.0	87.0	0.83		
	HB		85.7	85.7	0.86		
	NB		80.0	83.3	0.82		

network increases, so does the training time, but the accuracy decreases. In a comprehensive comparison, ResNet-18 has the highest validation accuracy and precision for each classification, recall, and F1-score. The verification accuracy and test accuracy rate are 90.5% and 91.0%, respectively. Although it is slightly lower than the VGG series network, the training time is 1/50 of it. As a result, ResNet-18 performs best in this experiment for the drainage hole target classification task.

**3.2. Comparison of Transfer Strategies.** In Section 3.1, the optimal network model ResNet-18 is obtained using transfer learning. This section continues to compare the performance of the model under different transfer strategies. Choose to freeze the weights of the different network layers by setting

the learning rate to zero. The parameters of the frozen layer will not be updated during training. Because the gradient of frozen layers does not need to be calculated, freezing the weights of multiple initial layers can significantly accelerate the network training time. If the new samples are small, freezing the shallower network layer also prevents those layers from overfitting the new samples. To test the advantages of transfer learning, the ResNet-18 network without pretraining was also used in this experiment.

ResNet-18 comprises 71 layers, including 8 residual boxes. In this experiment, the layer from the first to the layer behind each residual box is frozen sequentially, that is, layers 1–11 (after the first residual box), layers 1–18 (after the second residual box), layers 1–27 (after the third residual box), layers 1–34 (after the fourth residual box), layers 1–43

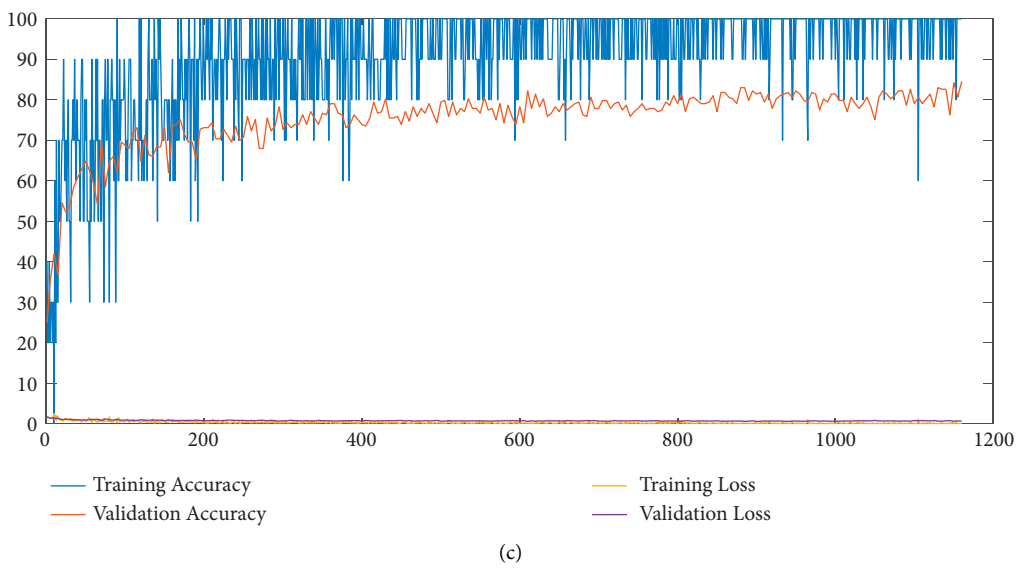
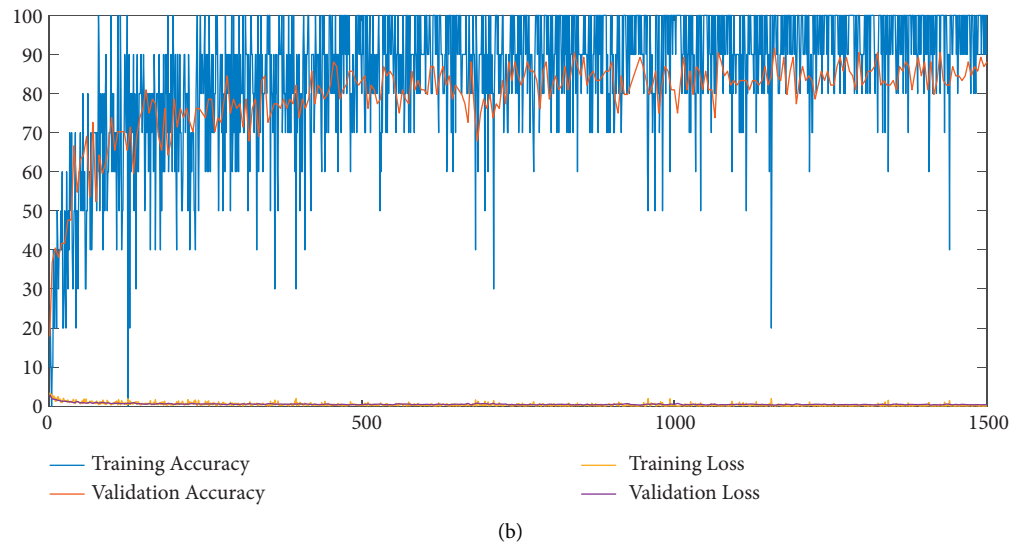
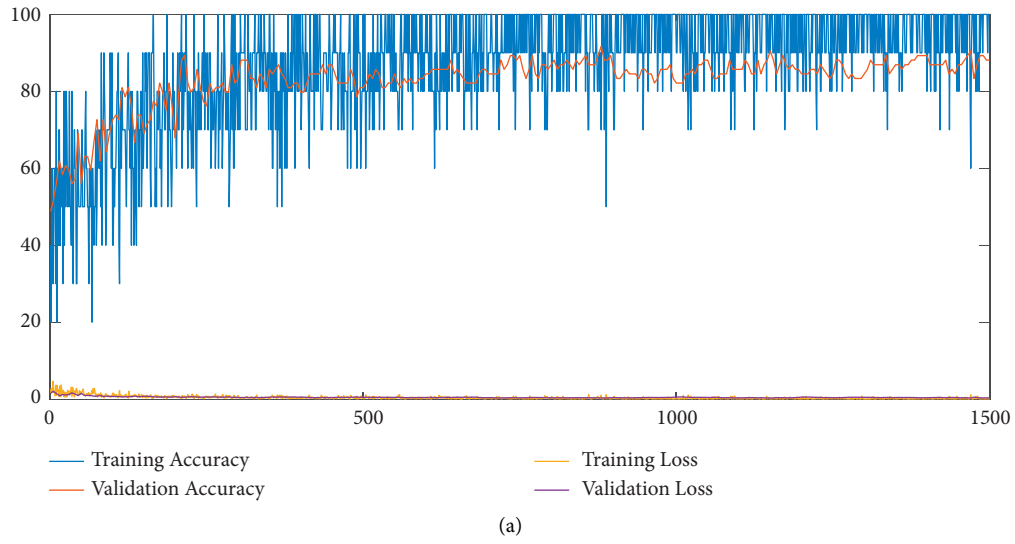
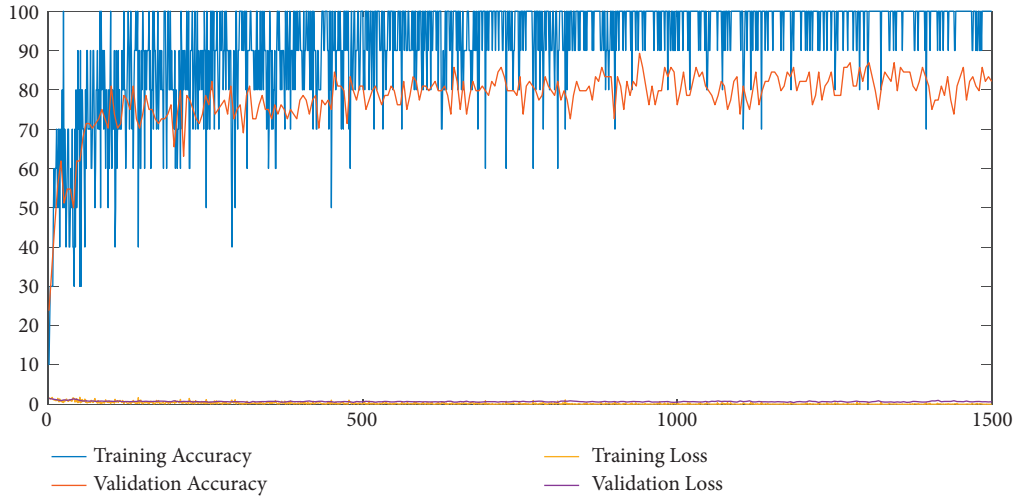
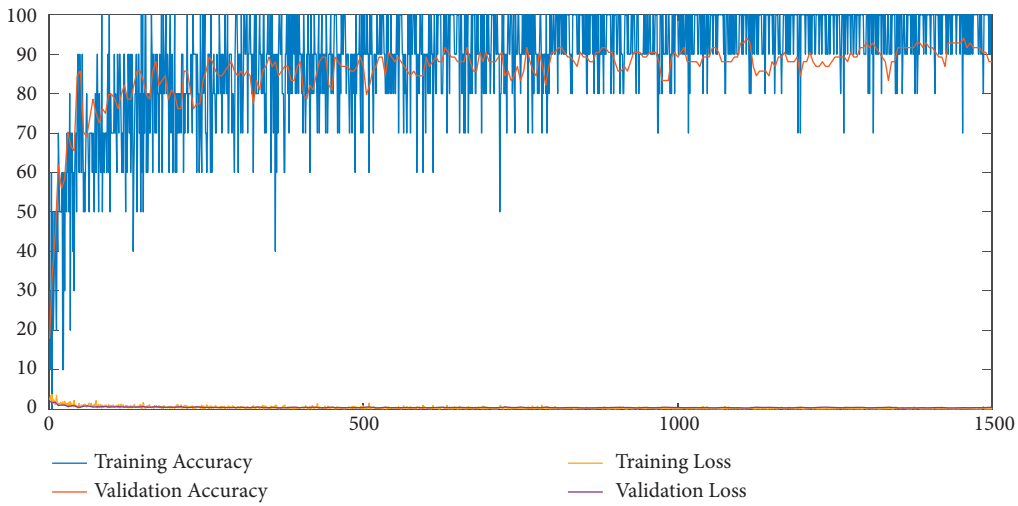


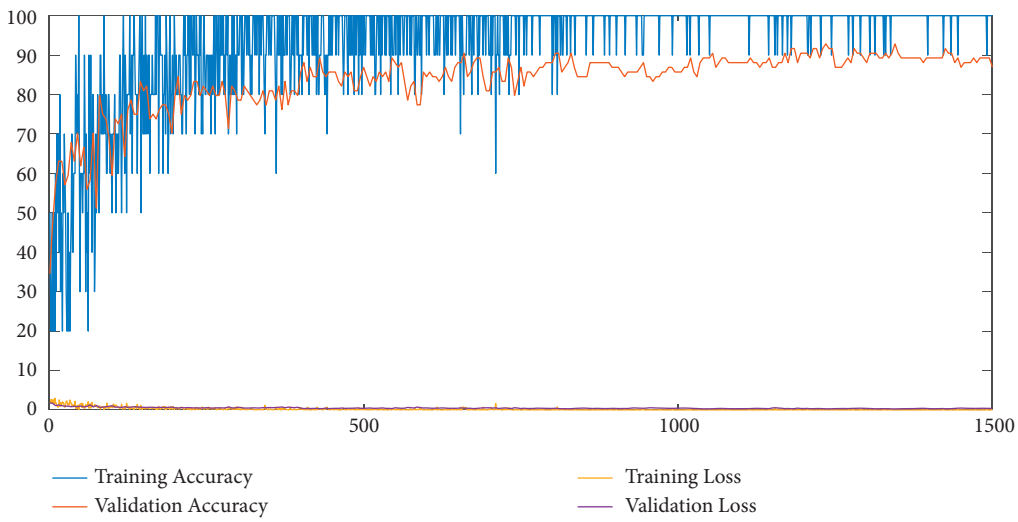
FIGURE 6: Continued.



(d)



(e)



(f)

FIGURE 6: Continued.



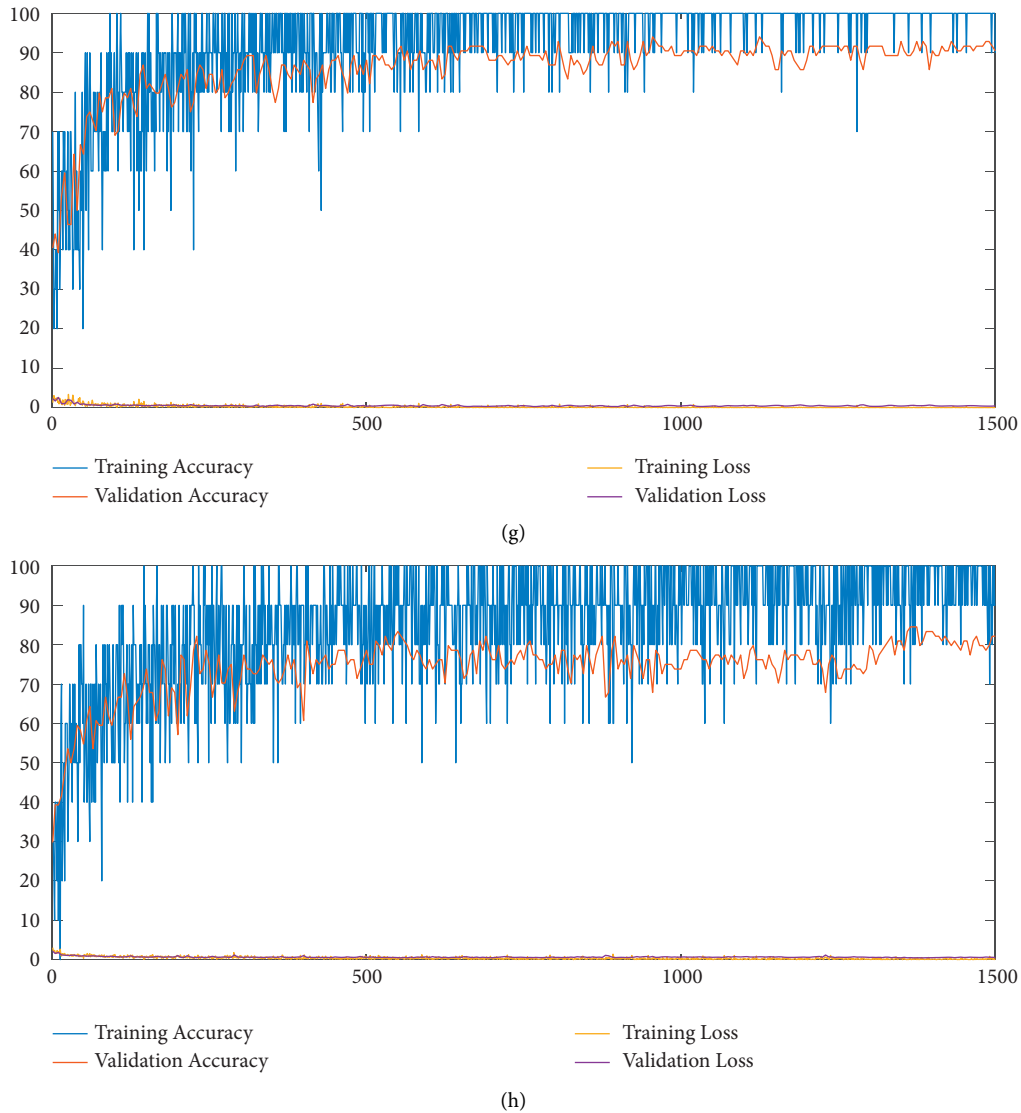


FIGURE 6: Accuracy and loss of different network models. (a)Accuracy and loss in the AlexNet training process. (b) Accuracy and loss in the ResNet-18 training process. (c) Accuracy and loss in the ResNet-50 training process. (d)Accuracy and loss in the ResNet-101 training process. (e)Accuracy and loss in the GoogLeNet training process. (f) Accuracy and loss in the VGG-16 training process. (g) Accuracy and loss in the VGG-19 training process. (h) Accuracy and loss in SqueezeNet training process.

(after the fifth residual box), layers 1–50 (after the sixth residual box), layers 1–59 (after the seventh residual box), and layers 1–66 (after the eighth residual box), respectively. The learning rate of the frozen layer is set to zero, all layers are reconnected in the original order, and the new layer diagram contains the same layers, but the learning rate of the frozen layer is zero.

The network models of different transfer strategies use the same network parameters. Table 2 presents the specific parameters. The recognition effects of the ResNet-18 using different transfer strategies are compared by freezing the networks of different layers. Table 4 presents the specific experimental comparison.

Through comparison, it is discovered that as the network freezing depth increases, the training time becomes shorter and shorter due to the fewer parameters that must be trained. When layers 1–11 are frozen, network validation accuracy and test accuracy suffer noticeably. When layers 1–18 are frozen, network verification accuracy is higher than that of training all layers of accuracy, but testing accuracy is lower. Network validation accuracy and test accuracy are significantly lower when layers 1–27 are frozen, but verification accuracy and evaluation indexes of the network are the highest when layers 1–34 are frozen, with validation accuracy and test accuracy of 91.7% and 90.0%, respectively. Following that, as the number of frozen layers increases, the

TABLE 4: ResNet-18 different transfer policy comparison.

Transfer strategy	Classify	Accuracy (ACC)	Precision (PPV) (%)	Recall (TPR) (%)	F 1-score (%)	Test accuracy (%)	Time
Train all layers	SB	90.5	93.1	90.0	0.92	91.0	8 m 40 s
	MB		91.3	91.3	0.91		
	HB		71.4	71.4	0.71		
	NB		92.0	95.8	0.94		
Freeze 1–11 layers after first residual module	SB	82.1	79.3	76.6	0.78	87.1	8 m 5 s
	MB		89.5	73.9	0.81		
	HB		85.7	85.7	0.86		
	NB		79.3	95.8	0.87		
Freeze 1–18 layers after second residual module	SB	92.9	90.0	100.0	0.95	86.1	7 m 33 s
	MB		100.0	82.6	0.90		
	HB		85.7	85.7	0.86		
	NB		92.0	95.8	0.94		
Freeze 1–27 layers after third residual module	SB	83.3	81.8	90.0	0.86	86.1	7 m 21 s
	MB		83.3	65.2	0.73		
	HB		75.0	85.7	0.80		
	NB		88.0	91.7	0.90		
Freeze 1–34 layers after fourth residual module	SB	91.7	96.4	90.0	0.93	90.0	7 m 3 s
	MB		91.3	91.3	0.91		
	HB		100.0	85.7	0.92		
	NB		85.2	95.8	0.90		
Freeze 1–43 layers after fifth residual module	SB	81.0	74.4	96.7	0.84	80.0	7 m 9 s
	MB		100.0	60.9	0.76		
	HB		55.6	71.4	0.63		
	NB		90.9	83.3	0.87		
Freeze 1–50 layers after sixth residual module	SB	81.0	78.8	86.7	0.83	88.1	6 m 35 s
	MB		88.9	69.6	0.78		
	HB		75.0	85.7	0.80		
	NB		80.0	83.3	0.82		
Freeze 1–59 layers after seventh residual module	SB	78.6	69.8	100.0	0.82	78.2	6 m 7 s
	MB		84.6	47.8	0.61		
	HB		71.4	71.4	0.71		
	NB		95.2	83.3	0.89		
Freeze 1–66 layers after eighth residual module	SB	69.1	66.7	80.0	0.73	69.3	5 m 33 s
	MB		63.2	52.2	0.57		
	HB		63.6	100.0	0.78		
	NB		83.3	62.5	0.71		
Untrained network	SB	64.3	54.2	86.7	0.67	58.4	8 m 52 s
	MB		73.3	47.8	0.58		
	HB		71.4	71.4	0.71		
	NB		85.7	50.0	0.63		

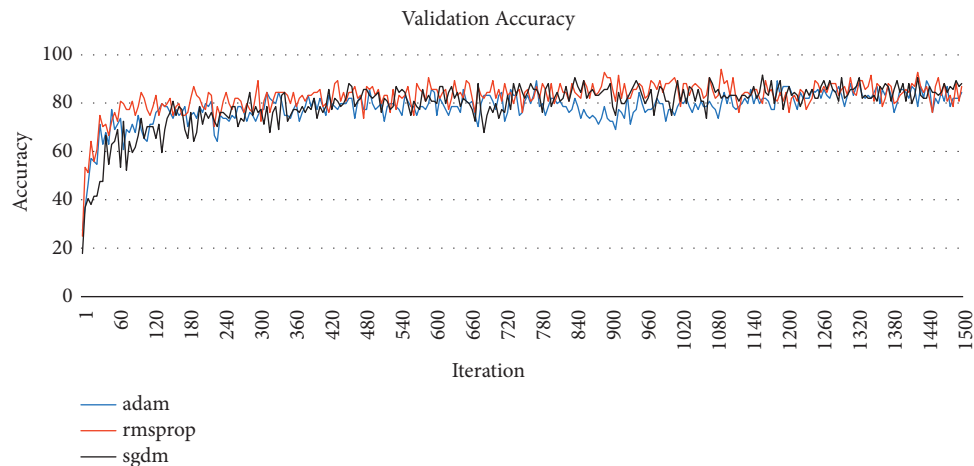


FIGURE 7: Validation accuracy of different solver models when the initial learning rate is 0.0001.

TABLE 5: ResNet-18 different model parameter comparison.

Solver name	Initial learn rate	Classify	Accuracy (ACC)	Precision (PPV)	Recall (TPR)	F1-Score (%)	Test accuracy (%)	Time
SGDM	0.01	SB	75.0%	69.4%	83.3	0.76	62.40	7 m 13 s
		MB		75.0%	52.2	0.62		
		HB		57.0%	42.9	0.49		
		NB		82.1%	95.8	0.88		
	0.001	SB	86.9%	78.4%	96.7	0.87	87.1	9 m 48 s
		MB		94.7%	78.3	0.86		
		HB		75.0%	85.7	0.80		
		NB		100.0%	83.3	0.91		
	0.0001	SB	91.7%	96.4%	90.0	0.93	90.0	7 m 3 s
		MB		91.3%	91.3	0.91		
		HB		100.0%	85.7	0.92		
		NB		85.2%	95.8	0.90		
Adam	0.01	SB	75.0%	60.0%	90.0	0.72	71.3	7 m 58 s
		MB		100.0%	65.2	0.79		
		HB		100.0%	85.7	0.00		
		NB		83.3%	65.2	0.73		
	0.001	SB	84.5%	89.7%	86.7	0.88	83.2	8 m 7 s
		MB		85.7%	78.3	0.82		
		HB		50.0%	71.4	0.59		
		NB		91.7%	91.7	0.92		
	0.0001	SB	83.3%	80.0%	80.0	0.80	91.0	7 m 45 s
		MB		80.0%	87.0	0.83		
		HB		77.8%	100.0	0.88		
		NB		95.0%	79.2	0.86		
RMSProp	0.01	SB	47.6%	41.7%	100.0	0.59	47.5	7 m 46 s
		MB		100.0%	4.3	0.08		
		HB		100.0%	28.6	0.44		
		NB		77.8%	29.2	0.42		
	0.001	SB	79.8%	84.8%	93.3	0.89	85.1	7 m 37 s
		MB		95.2%	87.0	0.91		
		HB		87.5%	100.0	0.93		
		NB		95.5%	87.5	0.91		
	0.0001	SB	85.7%	79.4%	90.0	0.84	93.0	7 m 30
		MB		82.6%	82.6	0.83		
		HB		85.7%	85.7	0.86		
		NB		100.0%	83.3	0.91		
Solver name	Initial learn rate	Classify	AP	mAP				
SGDM	0.01	SB	57.81%	50.02%				
		MB	39.15%					
		HB	24.45%					
		NB	78.65%					
	0.001	SB	75.81%	74.38%				
		MB	74.15%					
		HB	64.28%					
		NB	83.30%					
	0.0001	SB	86.76%	84.36%				
		MB	83.36%					
		HB	85.70%					
		NB	81.62%					

TABLE 5: Continued.

Solver name	Initial learn rate	Classify	Accuracy (ACC)	Precision (PPV)	Recall (TPR)	F1-Score (%)	Test accuracy (%)	Time
Solver name	Initial learn rate	Classify	AP	mAP				
Adam	0.01	SB	54.00%	64.80%				
		MB	65.20%					
		HB	85.70%					
	0.001	NB	54.31%					
		SB	77.77%					
		MB	67.10%	66.17%				
	HB	35.70%						
	NB	84.09%						
	0.0001	SB	64.00%					
MB		69.60%	71.66%					
HB		77.80%						
NB	75.24%							
RMSProp	0.01	SB	41.70%	24.33%				
		MB	4.30%					
		HB	28.60%					
	0.001	NB	22.72%					
		SB	79.12%					
		MB	82.82%	83.25%				
	HB	87.50%						
	NB	83.56%						
	0.0001	SB	71.46%					
MB		68.23%	74.11%					
HB		73.44%						
NB	83.30%							

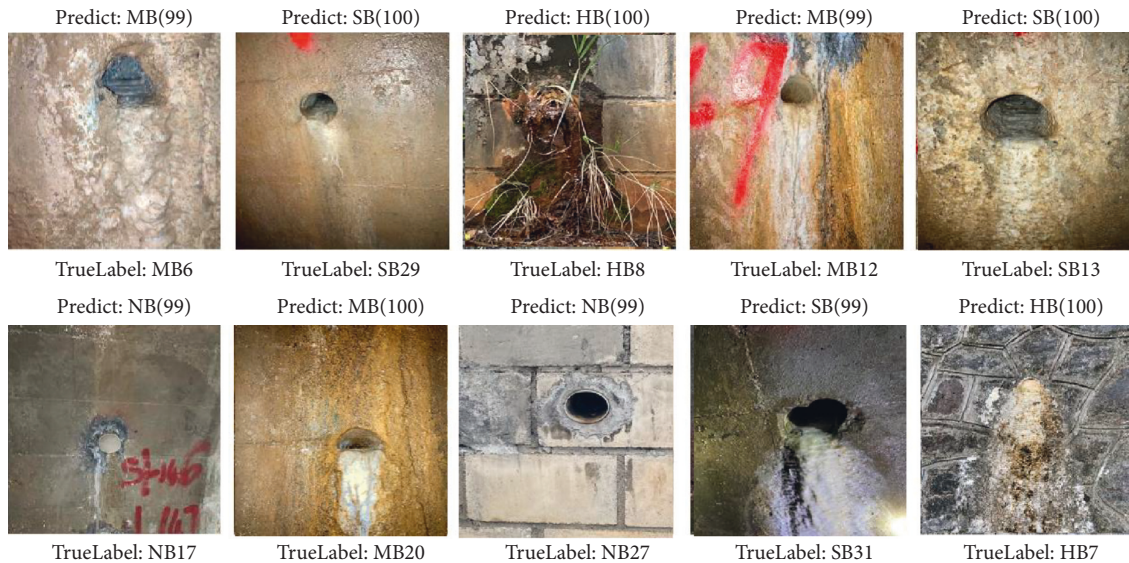


FIGURE 8: Test results.

accuracy of the network model gradually decreases. Furthermore, the network without pretraining is compared. The results show that, for the same number of training rounds, the training time of the network without pretraining is comparable to that of the network with pretraining for all layers. However, the accuracy is far lower than that of the pretrained network.

**3.3. Comparison of Model Parameters.** In the previous section, different migration strategies were compared, among which ResNet-18 frozen layers 1–34 performed best. Based

on this, we compared the prediction effects using three different solvers (Adam, SGDM, and RMSProp) when the model's initial learning rate was 0.01, 0.001, and 0.0001, respectively. Figure 7 shows the validation accuracy of different solver models when the initial learning rate is 0.0001. As presented in Table 5, the model accuracy improves dramatically when the learning rate decreases, and at the same learning rate, Adam outperforms RMSProp while SGDM outperforms Adam. When the solver is SGDM, the model verification accuracy is the highest (91.7%); when the learning rate is 0.0001, the test accuracy ranks third at 90.0%,

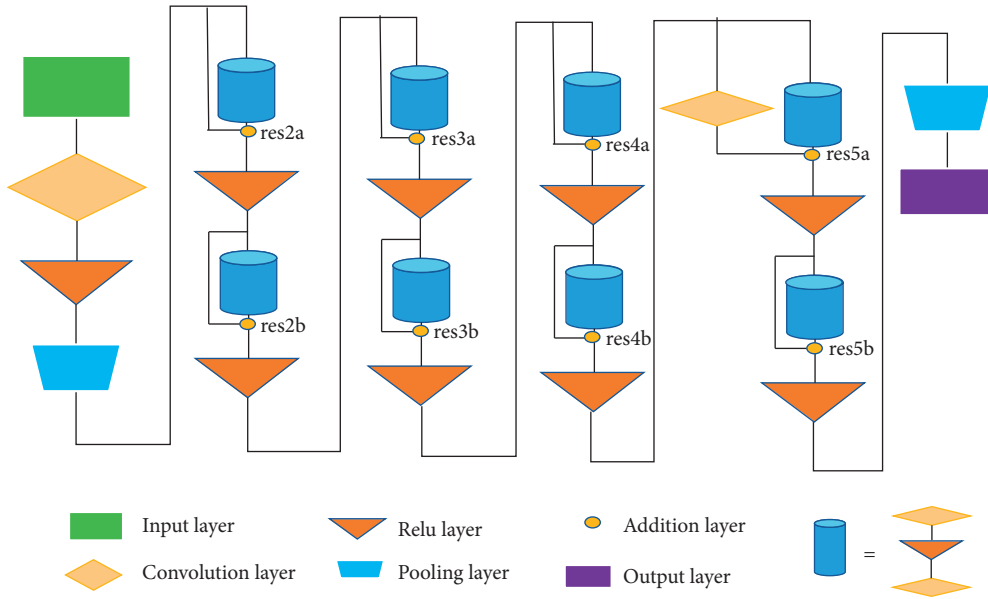


FIGURE 9: Frozen layer of ResNet-18.

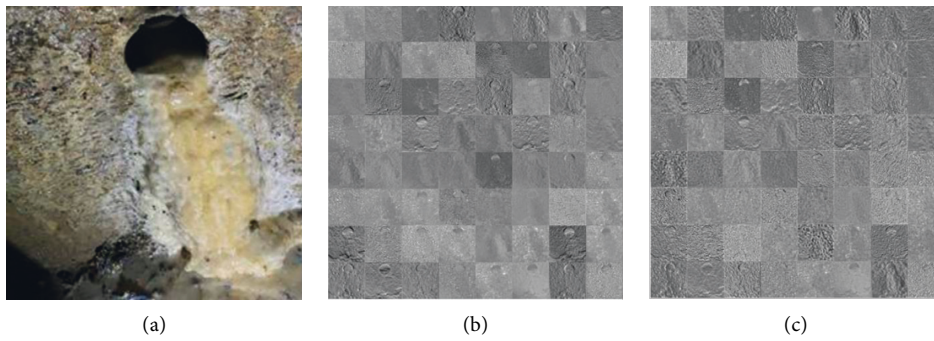
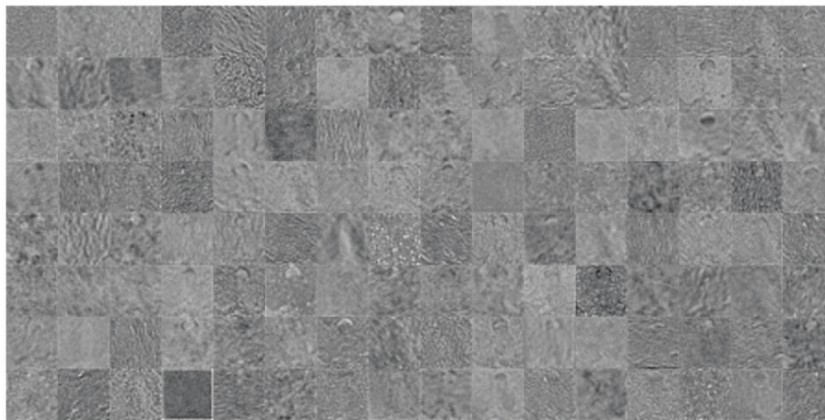


FIGURE 10: Feature images of res2a and res2b. (a) Raw image; (b) feature images of res2a (64 images); (c) feature images of res2b (64 images).



(a)  
FIGURE 11: Continued.



(b)

FIGURE 11: Feature images of res3a and res3b. (a) Feature images of res3a (128 images); (b) feature images of res3b (128 images).

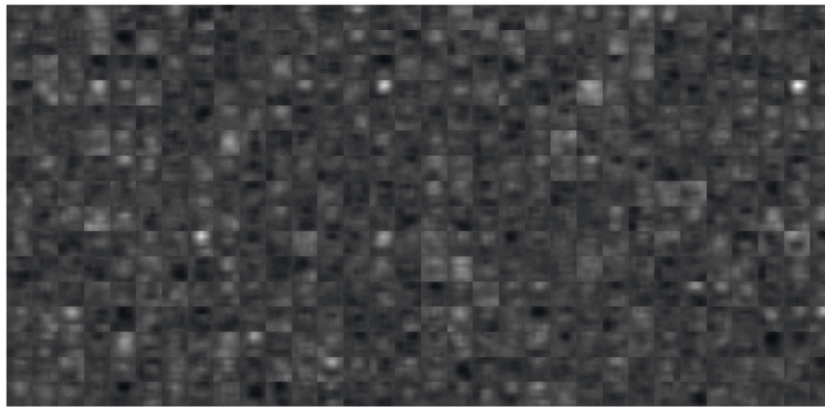


FIGURE 12: Feature images of res5b.

and other evaluation indexes are optimal. Figure 8 shows partial test results; the values in parentheses are the predicted confidence.

**3.4. Visualisation of Features.** This section shows how to feed images to ResNet-18 CNN and the activation region of the addition layer (res2a, res2b, res3a, res3b, and res5b) at the end of the first 1–4 and the last residual box of the network in Figure 9, observing which regions in the convolutional layers are activated on the image and comparing them with the corresponding regions in the original image to investigate the features. When comparing the activated regions with the original image, it was discovered that the channels in the shallower layers learn simple features such as colour and edges, while the channels in the deeper layers learn complex features.

Each layer of a CNN consists of several two-dimensional arrays called channels. Each block in the activation region grid is the output channel in the conv1 layer. White pixels indicate strong positive activation regions, and black pixels indicate strong negative activation regions. Primarily grey channels are not strongly activated for the input image. The pixel positions in the channel activation regions correspond to the same positions in the original image. A

white pixel at a position in a channel indicates that the channel is strongly activated at that position. Figure 10 shows the 64 feature maps obtained for each layer of res2a and res2b. Some of the channel images show the contours of the drainage holes.

Figure 11 shows the feature images of res3a and res3b, with 128 feature images obtained for each layer. Compared with res2a and res2b, the convolution process reduces the resolution of the feature images. Some additional interference was filtered out. The ideal features of the drainage holes were extracted from some of the feature images. Figure 12 shows the feature images for the last residual box addition layer, res5b, with 512 feature images obtained for each layer. At this point, the resolution continues to decrease, the image becomes extremely blurred, and the visual features disappear.

## 4. Conclusion and Outlook

Based on the drainage hole image samples, eight different pretrained CNN models, that is, AlexNet, SqueezeNet, VGG-16, VGG-19, GoogLeNet, ResNet-18, ResNet-50, and ResNet-101, were compared. The performance of the same model under different migration strategies and different

hyperparameters is compared. The ideal network model of blockage detection of drainage holes is obtained. Through the analysis of the experiment, the following conclusions are drawn.

- (1) Based on the drainage hole blockage samples, eight different pretraining network models were compared, and a relatively accurate (91.5%) drainage hole blockage detection network model based on ResNet-18 was trained, resulting in the classification of drainage hole blockage into four types based on degree, that is, slight blockage, moderate blockage, heavy blockage, and no blockage.
- (2) Compared with the transfer learning model, it takes much longer to retrain the network, and the network accuracy is much lower. Comparing the performance of the network model under different migration strategies, the training time decreases as the frozen layer increases. When selecting the appropriate relative shallow network to freeze, keeping the basic without accuracy reduction can decrease the network training time. However, after a certain depth, the accuracy of the model decreases as the number of frozen layers increases.
- (3) In this paper, we compare different solvers and initial learning rates of the network model, and the results show that as the learning rate decreases, the model accuracy significantly increases. For these experimental samples, the model accuracy is best when the initial learning rate is 0.0001 and the solver is SGDM.

The congestion classification network model is helpful for the detection and maintenance of drainage holes in public infrastructure. Detection personnel can consider using an unmanned aerial vehicle to collect drainage hole pictures according to the planned route and then input the collected pictures into the drainage hole blockage detection model, which can automatically classify the blockage degree of the drainage hole.

The target of the image differs greatly from the background in the actual image acquisition process due to factors such as shooting angle and drainage hole location, and the adaptability of the model is reduced, resulting in the correctness of the trained model in this paper. An improvement is still required compared with the application of deep learning in other aspects. In this paper, only the target classification is carried out for the degree of drainage hole blockage, and the detection and positioning of the disease location can be carried out based on this research. Using the target detection method, several types of diseases can be identified in a single image, and the research on this drainage hole blockage classification network model is of great importance for the maintenance of drainage pipes. Furthermore, it provides important technical support for the development of intelligent maintenance management systems for drainage pipes at a later stage.

## Data Availability

The data used to support the findings of this study are included within the article and are available from the corresponding author upon request.

## Conflicts of Interest

The authors declare that they have no conflicts of interest.

## Acknowledgments

The authors acknowledge the financial support provided by the Guangdong Provincial Natural Science Foundation of China (Grant no. 2019A1515011397).

## References

- [1] Y. Liu, C. A. Tang, P. Y. Wang, Y. P. Guan, and S. H. Wang, "Study on disease mechanism and theoretical quantification method of tunnel structure," *Advances in Civil Engineering*, vol. 2019, Article ID 4398524, 1–14 pages, 2019.
- [2] C. Gao, L. Xiang, and X. Zhang, *Lining Stress Caused by Crystal Lization Clogging of Tunnel Drainage Pipe at Different Water Levels*, Journal of Chongqing Jiaotong University, China, 2019.
- [3] C. L. Gao, S. C. Li, and C. J. Lin, "Development and application of model test system for water leakage disease in tunnel lining," *Rock and Soil Mechanics*, vol. 40, no. 4, pp. 1614–1622, 2019.
- [4] S. Y. Liu, F. Gao, and X. F. Zhang, "Experimental study on anti-crystallization law of tunnel transverse flocking drainpipe at different velocities," *Asia-Pacific Journal of Chemical Engineering*, vol. 15, 2020.
- [5] S. Y. Liu, X. F. Zhang, Y. F. Zhou, and F. Gao, "Optimization study of fluffy materials flocking drainage pipes to resist blockage based on MD binding energy," *Coatings*, vol. 11, no. 7, p. 853, 2021.
- [6] S. Fekri-Ershad and F. Tajeripour, "Multi-resolution and noise-resistant surface defect detection approach using new version of local binary patterns," *Applied Artificial Intelligence*, vol. 31, no. 5-6, pp. 395–410, 2017.
- [7] A. Ebrahimkhanlou, A. Farhidzadeh, and S. Salamone, "Multifractal analysis of crack patterns in reinforced concrete shear walls," *Structural Health Monitoring*, vol. 15, no. 1, pp. 81–92, 2016.
- [8] H. N. Ho, J. H. Lee, Y. S. Park, and L. Jong-Jae, "A synchronized multipoint vision-based system for displacement measurement of civil infrastructures," *The Scientific World Journal*, vol. 2021, Article ID 519146, 9 pages, 2012.
- [9] X. W. Ye, Y. Q. Ni, T. T. Wai, K. Wong, X. Zhang, and F. Xu, "A vision-based system for dynamic displacement measurement of long-span bridges: algorithm and verification," *Smart Structures and Systems*, vol. 12, no. 3\_4, pp. 363–379, 2013.
- [10] X. W. Ye, C. Z. Dong, and T. Liu, "Image-based structural dynamic displacement measurement using different multi-object tracking algorithms," *Smart Structures and Systems*, vol. 17, no. 6, pp. 935–956, 2016.
- [11] D. Ziou and S. Tabbone, *Edge Detection Techniques: An Overview*, 1998.

- [12] K. Rana and K. Mohamed, "Classification and analysis of deep learning applications in construction: a systematic literature review," *Automation in Construction*, vol. 129.
- [13] Z. Lingxin, S. Junkai, and Z. Baijie, "A review of the research and application of deep learning-based computer vision in structural damage detection," *Earthquake Engineering and Engineering Vibration*, vol. 21, no. 1, p. 1, 2022.
- [14] C. M. Yeum and S. J. Dyke, "Vision-based automated crack detection for bridge inspection," *Computer-Aided Civil and Infrastructure Engineering*, vol. 30, no. 10, pp. 759–770, 2015.
- [15] K. Makantasis, K. Karantzas, A. Doulamis, and N. Doulamis, "Deep supervised learning for hyperspectral data classification through convolutional neural networks," in *Proceedings of the IEEE International Geoscience and Remote Sensing Symposium (IGARSS)*, Milan, ITALY, July 2015.
- [16] Y. J. Cha, W. Choi, and O. Buyukozturk, "Deep learning-based crack damage detection using convolutional neural networks," *Computer-Aided Civil and Infrastructure Engineering*, vol. 32, no. 5, pp. 361–378, 2017.
- [17] Y. Xu, S. L. Li, D. Y. Zhang et al., "Identification framework for cracks on a steel structure surface by a restricted Boltzmann machines algorithm based on consumer-grade camera images," *Structural Control and Health Monitoring*, vol. 25, no. 2, Article ID e2075, 2018.
- [18] F. C. Chen and M. R. Jahanshahi, "NB-CNN: deep learning-based crack detection using convolutional neural network and naïve bayes data fusion," *IEEE Transactions on Industrial Electronics*, vol. 65, no. 5, pp. 4392–4400, 2018.
- [19] Y. Q. Bao, Z. Y. Tang, H. Li, and Y. Zhang, "Computer vision and deep learning-based data anomaly detection method for structural health monitoring," *Structural Health Monitoring*, vol. 18, no. 2, pp. 401–421, 2019.
- [20] I. Konovalenko, P. Maruschak, and V. Brevus, "Steel surface defect detection using an ensemble of deep residual neural networks," *Journal of Computing and Information Science in Engineering*, vol. 22, no. 1, 2022.
- [21] Y. Xue, F. Jia, and X. Cai, *An Optimization Strategy to Improve the Deep Learning-Based Recognition Model of Leakage in Shield Tunnels*, 2021.
- [22] J. C. P. Cheng and M. Wang, "Automated detection of sewer pipe defects in closed-circuit television images using deep learning techniques," *Automation in Construction*, vol. 95, pp. 155–171, 2018.
- [23] S. I. Hassan, L. M. Dang, I. Mehmood et al., "Underground sewer pipe condition assessment based on convolutional neural networks," *Automation in Construction*, 2019.
- [24] Q. Q. Zhou, Z. X. Situ, S. Teng, and G. Chen, "Convolutional neural networks-based model for automated sewer defects detection and classification," *Journal of Water Resources Planning and Management*, vol. 147, no. 7, 2021.
- [25] D. E. Rumelhart, G. E. Hinton, and R. J. J. N. Williams, "Learning representations by back propagating errors," *Nature*, vol. 323, no. 6088, pp. 533–536, 1986.
- [26] A. Krizhevsky, I. Sutskever, and G. Hinton, "ImageNet classification with deep convolutional neural networks," *Advances in Neural Information Processing Systems*, vol. 25, no. 2, 2012.
- [27] F. N. Iandola, S. Han, and M. W. Moskewicz, *SqueezeNet: AlexNet-level Accuracy with 50x Fewer Parameters and <0, 5MB model size*, 2016.
- [28] K. Simonyan and A. Zisserman, "Very deep convolutional networks for large-scale image recognition," *Computer Science*, 2014.
- [29] K. He, X. Zhang, and S. Ren, "Deep residual learning for image recognition," *IEEE Computer Society*, 2016.
- [30] C. Szegedy, W. Liu, and Y. Jia, "Going deeper with convolutions," *IEEE Computer Society*, 2014.
- [31] Z. D. Chen, L. Deng, B. Y. Wang, G. Li, and Y. Xie, "A comprehensive and modularized statistical framework for gradient norm equality in deep neural networks," *IEEE Transactions on Pattern Analysis and Machine Intelligence*, vol. 44, no. 1, pp. 13–31, 2022.